

# Emergence and global spread of a multidrug-resistant, community-associated MRSA lineage from the Indian subcontinent

Steinig E.J.<sup>1,2</sup>, Duchene S.<sup>3</sup>, Robinson D.A.<sup>4</sup>, Monecke S.<sup>5,6,7</sup>, Yokoyama M.<sup>8</sup>, Laabei M.<sup>8</sup>, Slickers P.<sup>5,6</sup>, Andersson P.<sup>1</sup>, Williamson D.<sup>9</sup>, Kearns A.<sup>10</sup>, Goering R.<sup>11</sup>, Dickson E.<sup>12</sup>, Ehricht R.<sup>5,6</sup>, Ip M.<sup>13</sup>, O'Sullivan M.V.N.<sup>14</sup>, Coombs G.W.<sup>15</sup>, Petersen A.<sup>16</sup>, Brennan G.<sup>17</sup>, Shore A.C.<sup>18</sup>, Coleman D.C.<sup>18</sup>, Pantosti A.<sup>19</sup>, de Lencastre H.<sup>20,21</sup>, Westh H.<sup>22,23</sup>, Kobayashi N.<sup>24</sup>, Heffernan H.<sup>25</sup>, Strommenger B.<sup>26</sup>, Layer F.<sup>26</sup>, Weber S.<sup>27</sup>, Aamot H.<sup>28</sup>, Skakni L.<sup>29</sup>, Peacock S.J.<sup>30</sup>, Sarovich D.<sup>1,31</sup>, Giffard P.<sup>1,32</sup>, Harris S.<sup>33</sup>, Parkhill J.<sup>33</sup>, Massey R.C.<sup>34</sup>, Holden M.T.G.<sup>33,35</sup>, Bentley S.D.<sup>33</sup>, and Tong S.Y.C.<sup>1,36,\*</sup>

<sup>1</sup>Menzies School of Health Research, Darwin, Australia, <sup>2</sup>Australian Institute of Tropical Health and Medicine, Townsville, Australia, <sup>3</sup>Department of Biochemistry & Molecular Biology, University of Melbourne, Melbourne, Australia, <sup>4</sup>University of Mississippi Medical Center, Jackson, United States, <sup>5</sup>Abbott (Alere Technologies GmbH), Jena, Germany, <sup>6</sup>InfectoGnostics Research Campus, Jena, Germany, <sup>7</sup>Technical University of Dresden, Dresden, Germany, <sup>8</sup>Milner Centre for Evolution, University of Bath, Bath, United Kingdom, <sup>9</sup>Doherty Applied Microbial Genomics, Department of Microbiology & Immunology, The University of Melbourne at The Peter Doherty Institute for Infection and Immunity, Melbourne, Australia; Microbiological Diagnostic Unit Public Health Laboratory, Department of Microbiology & Immunology, The University of Melbourne at The Peter Doherty Institute for Infection and Immunity, Melbourne, Australia, <sup>10</sup>Public Health England, National Infection Service, London, United Kingdom, <sup>11</sup>Creighton University, Omaha, United States, <sup>12</sup>Scottish Microbiology Reference Laboratories, Glasgow, United Kingdom, <sup>13</sup>The Chinese University of Hong Kong, Hong Kong, <sup>14</sup>The University of Sydney, Sydney, Australia, <sup>15</sup>School of Veterinary and Laboratory Sciences, Murdoch University, Murdoch, Western Australia, <sup>16</sup>Statens Serum Institut, Copenhagen, Denmark, <sup>17</sup>National MRSA Reference Laboratory, St. James's Hospital, Dublin, Ireland, <sup>18</sup>Microbiology Research Unit, School of Dental Science, University of Dublin, Trinity College Dublin, Ireland, <sup>19</sup>Istituto Superiore di Sanità, Rome, Italy, <sup>20</sup>Instituto de Tecnologia Química e Biológica, Oeiras, Portugal, <sup>21</sup>The Rockefeller University, New York City, United States of America, <sup>22</sup>University of Copenhagen, Copenhagen, Denmark, <sup>23</sup>Hvidovre University Hospital, Hvidovre, Denmark, <sup>24</sup>Sapporo Medical University, Sapporo, Japan, <sup>25</sup>Institute of Environmental Science and Research, Wellington, New Zealand, <sup>26</sup>Robert Koch Institute, Wernigerode, Germany, <sup>27</sup>Sheikh Khalifa Medical City, Abu Dhabi, United Arab Emirates, <sup>28</sup>Akershus University Hospital, Lørenskog, Norway, <sup>29</sup>King Fahd Medical City, Riyadh, Kingdom of Saudi Arabia, <sup>30</sup>London School of Hygiene and Tropical Medicine, United Kingdom, <sup>31</sup>Sunshine Coast University, Sippy Downs, Australia, <sup>32</sup>The School of Psychological and Clinical Sciences, Charles Darwin University, Darwin, Australia, <sup>33</sup>Wellcome Trust Sanger Institute, Cambridge, United Kingdom, <sup>34</sup>School of Cellular and Molecular Medicine, University of Bristol, United Kingdom, <sup>35</sup>University of St Andrews, St Andrews, United Kingdom, <sup>36</sup>Victorian Infectious Disease Service, The Royal Melbourne Hospital, and The University of Melbourne, at the Peter Doherty Institute for Infection and Immunity, Melbourne, Australia

# **Abstract**

The global spread of antimicrobial resistance has been well documented in Gram-negative bacteria and healthcare-associated epidemic pathogens, often emerging from regions with heavy antimicrobial use. However, the degree to which similar processes occur with Gram-positive bacteria in the community setting is less well understood. Here we demonstrate the recent origin and global spread from the Indian subcontinent of a multidrug resistant *Staphylococcus aureus* lineage, sequence type 772 (Bengal Bay clone). Short-term outbreaks occurred following intercontinental transmission, typically associated with travel and family contacts, but ongoing endemic transmission was uncommon. Instrumental in the emergence of a single dominant clade in the early 1990s was the acquisition of a multidrug resistance integrated plasmid that did not appear to incur a significant fitness cost. The Bengal Bay clone therefore combines the multidrug resistance of traditional healthcare-associated clones with the epidemiological and virulence potential of community-associated clones.

# **Introduction**

Methicillin-resistant *Staphylococcus aureus* (MRSA) is a major human pathogen with a propensity to acquire antibiotic resistance, complicating treatment and allowing persistence in environments where there is antibiotic selection pressure. While multidrug resistance has traditionally been associated with healthcare-associated strains, the emergence of multidrug resistant MRSA that is capable of surviving in community reservoirs would pose a significant challenge to infection control and public health<sup>1</sup>. While previous studies have highlighted localized or sporadic emergence of multidrug resistant strains in the community setting<sup>2-7</sup>, there has so far been limited evidence for resistance acquisition driving the emergence and global dissemination of an epidemic, community-associated lineage of MRSA (as opposed with healthcare-associated lineages). Given the heavy burden and costs associated with MRSA infections<sup>8,9</sup>, there is an urgent need to elucidate the patterns and drivers of the spread of novel virulent and multidrug-resistant MRSA.

In 2004, a novel *S. aureus* clone designated sequence type (ST) 772 was isolated from hospitals in Bangladesh<sup>10</sup> and from a community-setting in India<sup>11</sup>. The clone continued to be reported in community- and healthcare-associated environments in India, where it has become one of the dominant epidemic lineages of community-associated MRSA<sup>12</sup>. Similar to other *S. aureus*, ST772 primarily causes skin and soft tissue infections, but more severe manifestations such as bacteraemia and necrotising pneumonia have been observed. Its potential for infiltration into nosocomial

environments<sup>13–16</sup> and resistance to multiple classes of commonly used antibiotics (aminoglycosides,  $\beta$ -lactams, fluoroquinolones, macrolides and trimethoprim)<sup>16–18</sup> has resulted in ST772 becoming a serious public health concern in South Asia and elsewhere. Over the last decade, the clone has been isolated from community- and hospital-environments in Asia, Australasia, Africa, the Middle East and Europe (Supplementary Map 1, Supplementary Table 1). As a consequence of its discovery, distribution and epidemiology, the lineage has been informally dubbed the “Bengal Bay clone”<sup>19</sup>. Despite clinical and epidemiological hints for a recent and widespread dissemination of ST772, a unified perspective on the global evolutionary history and emergence of the clone is lacking.

Here, we analyse whole genome sequences from a globally representative collection of 340 ST772 strains to elucidate the key events associated with the emergence and global spread of a multidrug resistant community-associated MRSA clone. We found that international travel and family connections to the Indian subcontinent were closely linked with the global spread of ST772. The integration of a multidrug resistance plasmid led to the emergence of a dominant clade (ST772-A) in the early 1990s with phenotypic assays suggesting that the mobile element has not incurred a significant fitness cost to this clade.

## **Results**

We generated whole genome sequence data of 354 *S. aureus* ST772 isolates collected across Australasia, South Asia, Hong Kong, the Middle East and Europe between 2004 and 2013 (Supplementary Map 2, Supplementary Table 2). Fourteen isolates were excluded after initial quality control due to contamination (Supplementary Tables 2, 3). The remainder mapped with 165x average coverage against the PacBio reference genome DAR4145<sup>18</sup> from Mumbai (Supplementary Tables 2, 3). Phylogenetic analysis using core-genome SNPs ( $n = 7,063$ ) revealed little geographic structure within the lineage (Figure 1a). Eleven ST772 methicillin-susceptible *S. aureus* (MSSA) and -MRSA strains were basal to a single globally distributed clade (ST772-A,  $n = 329$ ) that harbored an integrated resistance plasmid (IRP) described in the reference genome DAR4145<sup>18</sup> (Figures 1a, 1b). Population network analysis distinguished three distinct subgroups within ST772-A (Figures 1a, 1c): an early-branching subgroup harboring multiple subtypes of the staphylococcal chromosome cassette (SCCmec) (A1,  $n = 81$ ), a dominant subgroup (A2,  $n = 153$ ) and an emerging subgroup (A3,  $n = 56$ ), that exclusively harbors a short variant of SCCmec-V.

## Emergence and global spread from the Indian subcontinent

Epidemiological and genomic characteristics of ST772 were consistent with an evolutionary origin from the Indian subcontinent. Sixty percent of isolates in this study were collected from patients with family- or travel-background in Bangladesh, India, Nepal or Pakistan, compared to unknown (19%) or other countries (21%) (Figure 2a, Supplementary Table 2). We found significantly more isolates from India and Bangladesh among the basal strains, compared to clade ST772-A (Fisher's exact test, 5/11 vs. 47/291,  $p = 0.026$ ). In particular, three isolates from India and Bangladesh were basal in the (outgroup-rooted) maximum-likelihood phylogeny (Figure 1b, Supplementary Figure 1), including two MSSA samples from the original isolations in 2004 (RG28, NKD22). Isolates recovered from South Asia were genetically more diverse than isolates from Australasia and Europe, supporting an origin from the Indian subcontinent (Figure 2b, Supplementary Figure 2).

Consistent with a methicillin-susceptible progenitor, a significantly higher proportion of MSSA was found in the basal isolates (Fisher's exact test, 4/11 vs. 31/291,  $p = 0.028$ ) and MSSA isolates demonstrated a lower patristic distance to the root of the maximum likelihood phylogeny compared to MRSA (Supplementary Figure 3a). Although it appears that MSSA is proportionately more common in South Asia (Supplementary Figure 3b), it is also possible that the observed distribution may be related to non-structured sampling.

Phylogenetic dating suggests an initial divergence of the ancestral ST772 population in 1970 (age of root node: 1970.02, CI: 1955.43 – 1982.60) with a core-genome substitution rate of  $1.61 \times 10^{-6}$  substitutions/site/year after removing recombination (Figure 2c, 2d, Supplementary Figures 4, 5). This was followed by the emergence of the dominant clade ST772-A and its population subgroups in the early 1990s (ST772-A divergence, 1990.83, 95% CI: 1980.38 – 1995.08). The geographic pattern of dissemination is heterogeneous (Figure 1a). There was no evidence for widespread endemic dissemination of the clone following intercontinental transmission, although localised healthcare-associated outbreak clusters occurred in neonatal intensive care units in Ireland (NICU-1 and NICU-2, Figure 1a, Supplementary Figure 6)<sup>20</sup> and have been reported from other countries in Europe<sup>16</sup> and South Asia<sup>13–15</sup>. While some localised spread in the community was observed among our isolates, patients in local transmission clusters often had traveled to or had family in South Asia (19/27 clusters, Supplementary Figure 6).

# **Antibiotic resistance acquisition is associated with emergence and dissemination**

We examined the distribution of virulence factors, antibiotic resistance determinants and mutations in coding regions to identify the genomic drivers in the emergence and dissemination of ST772. Nearly all isolates (336/340) carried the Panton-Valentine leucocidin (PVL) genes *lukS/F*, most isolates (326/340) carried the associated enterotoxin A (*sea*) and all isolates carried *scn* (Supplementary Table 5). This indicates a nearly universal carriage, across all clades, of both, a truncated *hly*-converting prophage (the typically associated staphylokinase gene *sak* was only present in one isolate) and the PVL/*sea* prophage  $\phi$ -IND772<sup>21</sup>. Amongst other virulence factors, the enterotoxin genes *sec* and *sel*, the gamma-hemolysin locus, *egc* cluster enterotoxins and the enterotoxin homologue ORF CM14 were ubiquitous in ST772 (Supplementary Table 7). We detected no statistically significant difference between core virulence factors present in the basal group and ST772-A (Supplementary Table 5, Supplementary Figure 7).

We noted a pattern of increasing antimicrobial resistance as successive clades of ST772 emerged. Predicted resistance phenotypes across ST772 were common for ciprofloxacin (97.4%), erythromycin (96.2%), gentamicin (87.7%), methicillin (89.7%), penicillin (100%) and trimethoprim (98.8%), with a corresponding resistome composed of acquired and chromosomally encoded genes and mutations (Figure 3a, Figure 3b, Supplementary Table 6). There was significantly less predicted resistance in the basal strains compared to ST772-A, including overall multidrug-resistance ( $\geq 3$  classes, 8/11 vs. 291/291, Fisher's exact test,  $p < 0.001$ ) (Figure 3d). The key resistance determinants of interest were the SCC*mec* variants, an integrated resistance plasmid, and other smaller mobile elements and point mutations.

MRSA isolates predominantly harbored one of two subtypes of SCC*mec*-V: a short variant (5C2) or a composite cassette (5C2&5), which encodes a type 5 *ccr* complex containing *ccrC1* (allele 8) between the *mec* gene complex and *orfX*<sup>22</sup> (Supplementary Figure 8). Integration of the Tn4001 transposon encoding aminoglycoside resistance gene *aadA-aphD* occurred across isolates with different SCC*mec* types (260/267), but not in MSSA (0/35). All MRSA isolates ( $n = 7$ ) within the basal group carried the larger composite cassette SCC*mec*-V (5C2&5), with two of these strains lacking *ccrC* and one isolate carried a remnant of SCC*mec*-IV (Figure 1a).

The diversity of SCC*mec* types decreased as ST772-A diverged into subgroups (Figure 1a, c, Supplementary Table 6). ST772-A1 included MSSA ( $n = 30$ ) as well as SCC*mec*-V (5C2) ( $n = 22$ ) and (5C2&5) ( $n = 18$ ) strains. Four isolates harbored a putative composite SCC element that included

SCCmec-V (5C2), as well as *pls* and the *kdp* operon previously known from SCCmec-II. One isolate harbored a composite SCCmec-V (5C2&5) with copper and zinc resistance elements, known from the European livestock associated CC398-MRSA<sup>23</sup>. Another six isolates yielded irregular and/or composite SCC elements (Supplementary Table 6). In contrast, the dominant subgroups ST772-A2 and -A3 exclusively carried the short SCCmec-V (5C2) element. Eleven of these isolates (including all isolates in NICU-2) lacked *ccrC* and two isolates carried additional recombinase genes (*ccrA/B2* and *ccrA2*).

ST772-A was characterized by the acquisition of an integrated multidrug resistance plasmid (IRP, Figure 3c), encoding the macrolide-resistance locus *msrA* / *mphC*, as well as determinants against  $\beta$ -lactams (*blaZ*), aminoglycosides (*aadE-sat4-aphA3*) and bacitracin (*bcrAB*). Thus predicted resistance to erythromycin was uniquely found in ST772-A and not in any of the basal strains (Fisher's exact test, 289/291 vs 0/11,  $p < 0.001$ , Figure 3d). The mosaic IRP element was highly similar to a composite extrachromosomal plasmid in ST8 (USA300)<sup>24</sup> and a SCCmec integration in the J2 region of the ST80<sup>25</sup> reference genome (Figure 3c, Supplementary File 1). A search of closed *S. aureus* genomes ( $n = 274$ ) showed that the element is rare and predominantly plasmid-associated across ST8 genomes (6/274), with one chromosomal integration in the ST772 reference genome and the SCCmec integration in the ST80 reference genome (Supplementary Table 9).

Three basal strains were not multi-drug resistant and included two isolates from the original collections in India (RG28) and Bangladesh (NKD122) (Figure 1a, 3a). These two strains lacked the trimethoprim determinant *dfrG* and the fluoroquinolone mutations in *grrA* or *gyrA*, encoding only a penicillin-resistance determinant *blaZ* on a Tn554-like transposon. However, seven of the strains more closely related to ST772-A did harbor mobile elements and mutations conferring trimethoprim (*dfrG*) and quinolone resistance (*grrA* and *gyrA* mutations). Interestingly, we observed a shift from the quinolone resistance *grrA* S80F mutation in basal strains and ST772-A1, to the *grrA* S80Y mutation in ST772-A2 and -A3 (Figure 3a).

Thus, the phylogenetic distribution of the key resistance elements suggests acquisition of the IRP by a PVL-positive MSSA strain in the early 1990s (ST772-A1 divergence, 1990.83, 95% CI: 1980.38 – 1995.08), followed by fixation of both the shorter variant of SCCmec-V (5C2) and the *grrA* S80Y mutation in a PVL- and IRP-positive MSSA ancestor in the late 1990s (ST772-A2 divergence, 1999.18, 95% CI: 1993.26 – 2001.56) (Figure 1a, Figure 2c).



## Phenotypic comparison of basal strains and the derived ST772-A lineage

We found three other mutations of interest that were present exclusively in ST772-A strains (Supplementary Table 7). The first mutation caused a non-synonymous change in *fbpA* (L55P), encoding a fibrinogen-binding protein that mediates surface adhesion in *S. aureus*<sup>26</sup>. The second comprised a non-synonymous change (L67V) in the *plc* gene, encoding a phospholipase associated with survival in human blood cells and abscess environments in USA300<sup>27</sup>. The third encoded a non-synonymous mutation (S273G) in *tet(38)*, an efflux pump that promotes resistance to tetracyclines as well as survival in abscess environments and skin colonisation<sup>28</sup>. The functional implication of genes harboring these canonical mutations might suggest a modification of the clone's ability to colonise and cause SSTIs.

In light of these canonical SNPs, we selected five basal strains and 10 strains from ST772-A to screen for potential phenotypic differences that may contribute to the success of ST772-A. We assessed *in vitro* growth, biofilm formation, cellular toxicity, and lipase activity (Figure 4, Supplementary Table 8). We found no statistically significant differences between the basal strains and ST772-A in these phenotypic assays, apart from significantly lower lipase activity among ST772-A strains (Welch's two-sided t-test,  $t = 3.4441$ ,  $df = 6.0004$ ,  $p = 0.0137$ , Figure 4e), which may be related to the canonical non-synonymous mutation in *plc*. However, it is increased rather than decreased lipase activity that has been associated with viability of *S. aureus* USA300 in human blood and neutrophils<sup>27</sup>. We found no difference in the median growth rate of ST772-A compared to the basal strains (Figure 4, Mann-Whitney,  $W = 27$ ,  $p = 0.8537$ , Supplementary Table 8), although there were two ST772-A strains that grew more slowly suggesting the possibility of some strain to strain variability. However, overall, it appears that acquisition of resistance determinants on the IRP has not incurred a significant cost to *in vitro* growth of strains from ST772-A.

## Discussion

In this study, we used whole genome sequencing in combination with epidemiological and phenotypic data to investigate the drivers behind the emergence and spread of a multidrug resistant community-associated MRSA lineage from the Indian subcontinent. Our data suggests that the Bengal Bay clone has acquired the multidrug phenotype of traditional healthcare-associated MRSA, but retains the epidemiological and virulence potential of community-associated MRSA.

Within our dataset, the basal population of ST772 appears to have emerged from the Indian

203 subcontinent in the 1960s to early 1970s. This basal population included strains from the original  
204 isolations of ST772 in Bangladesh and India in 2004. Recent studies have detected ST772-MSSA and  
205 -MRSA in Nepal<sup>29</sup> and ST772-MRSA in Pakistan<sup>30</sup> also, but it is unclear whether the lineage has  
206 been endemic in these countries prior to its emergence in India. Deeper genomic surveillance of  
207 ST772-MSSA and -MRSA in the region will be necessary to understand the local epidemiology and  
208 evolutionary history of the clone on the Indian subcontinent.

209

210 The establishment and expansion of a single dominant clade (ST772-A) occurred in the early 1990s  
211 and was associated with the acquisition of an integrated multidrug resistance MGE. The element is  
212 similar to a previously described extrachromosomal plasmid of USA300<sup>24</sup> and a partially integrated  
213 element in the *SCCmec* of a ST80 reference genome<sup>25</sup>. While the element was found only once in  
214 the ST80 lineage<sup>31</sup> and occurs predominantly on plasmids in closed ST8 (USA300) genomes, its  
215 distribution and contribution to the emergence of resistance in the ST8 lineage has so far not been  
216 addressed<sup>32,33</sup>. In contrast, the ubiquitous occurrence and retention of the element in ST772-  
217 A suggests that it was instrumental to the emergence of the dominant clade in the Bengal Bay clone..  
218 Importantly, our phenotype assays show that acquisition of drug resistance on this element was not  
219 accompanied with a significant fitness cost to ST772-A. This raises the possibility that members of  
220 this clade will both survive in environments where antibiotics are heavily used, such as hospitals or  
221 in communities with poor antibiotic stewardship, but also be at little disadvantage in environments  
222 where there is less antibiotic use, because its growth rate is comparable to that of non-resistant strains.

223

224 Furthermore, we observed a replacement of the long composite *SCCmec*-V (5C2&5) element with  
225 the shorter *SCCmec*-V (5C2) and fixation of the quinolone resistance mutation from *grlA* S80F to the  
226 *grlA* S80Y as ST772 diverged into its population subgroups in the 1990s. In light of earlier studies  
227 demonstrating a fitness advantage in having a smaller *SCCmec* element<sup>34-36</sup>, the fixation of the shorter  
228 *SCCmec*-V (5C2) may be a contributing factor to the success of ST772. We speculate that these  
229 changes may have allowed the clone to retain its multidrug resistant phenotype without incurring a  
230 significant fitness cost. Further work is required to investigate the role of resistance dynamics in the  
231 evolution and fitness potential of ST772. While we only assayed for a limited number of phenotypic  
232 differences, our data suggest that acquisition of antibiotic resistance was a key driver in the emergence  
233 and persistence of ST772-A.

234

235 Given the available epidemiological data, phylogeographic heterogeneity and the clone's limited  
236 success to establish itself in regions outside its endemic range in South Asia (Figure 1a), there appears  
237 to be ongoing exportation of ST772 from the Indian subcontinent, associated with travel and family



background in the region. This is supported by reports of MRSA importation in travelers, including direct observations of ST772 importation by returnees from India<sup>37</sup>. Our data suggest non-endemic spread within households and the community, including short-term outbreaks at two NICUs in Ireland. This pattern of limited endemic transmission is supported by reports of small transmission clusters in hospitals and households during a comprehensive surveillance study of ST772 in Norway<sup>16</sup>. The rapid emergence, global exportation and patterns of local transmission, together with a relatively homogenous genotype, emphasize the clone's high transmissibility.

Overall, the pattern of spread mirrors other community-associated MRSA lineages such as USA300<sup>38,39</sup>, ST80-MRSA<sup>31</sup> and ST59<sup>6</sup> where clones emerge within a particular geographic region, are exported elsewhere, but rarely become established and endemic outside of their place of origin. In contrast, healthcare-associated MRSA clones such as CC22-MRSA-IV (EMRSA-15)<sup>40</sup> and ST239-MRSA-III<sup>41,42</sup> demonstrate much stronger patterns of phylogeographic structure, consistent with importation into a country followed by local dissemination through the healthcare system. The pattern of dissemination and potential for survival of multidrug resistant clones in environments outside healthcare settings, as demonstrated in this study, may have important implications for infection control of community-associated MRSA.

Considering the widespread use of antibiotics and associated poor antibiotic regulation, poor public health infrastructure, and high population density in parts of South Asia, the emergence and global dissemination of multidrug resistant bacterial clones (both Gram-positive and Gram-negative) is alarming, and perhaps not surprising. Here, we demonstrate that the acquisition of specific antimicrobial resistance determinants has been instrumental in the evolution and emergence of a multidrug resistant community-associated MRSA clone. Global initiatives and funding to monitor the occurrence of emerging clones and resistance mechanisms, and support for initiatives in antimicrobial stewardship at community, healthcare and agricultural levels are urgently needed.

# 264 **Figures**

265

266 **Figure 1:** Evolutionary history and population structure of ST772. **(a)** Maximum likelihood  
 267 phylogeny of ST772 (n = 340) based on 7,063 core-genome SNPs. Branch colors denote country of  
 268 isolation, the inner ring delineates presence and type of *SCCmec*, the middle ring shows presence of  
 269 the integrated resistance plasmid and the outer ring denotes community-membership of the population  
 270 graph shown in (c). Communities match the tree topology, with several basal isolates (n = 11) and a  
 271 single derived clade ST772-A (n = 329) composed of three population subgroups (A1 – A3). Isolates  
 272 from two outbreaks in neonatal intensive care units in Ireland are indicated in grey (NICU-1 and  
 273 NICU-2). Only one representative isolate from longitudinal sampling of a single healthcare worker  
 274 (n = 39) is included (red circle). **(b)** Basal strains of ST772 showing positions of isolates from India  
 275 and Bangladesh at the root of the phylogeny (RG28, DAR4066, NKD122). **(c)** Population graph based  
 276 on pairwise SNP distances, showing *SCCmec* type (node color as for Figure 1a legend) and  
 277 population subgroups (polygons, A1-A3). Dashed circles denote hospital-associated outbreaks in  
 278 Ireland (NICU-1 and NICU-2).

279

280 **Figure 2:** Molecular epidemiology of ST772. **(a)** Patient family- or travel-background in South Asia  
 281 (India, Pakistan, Nepal, Bangladesh) (59.5%, purple), other countries (21.2%, green) or unknown  
 282 status (19.3%, gray), is widely distributed across the phylogenetic topology of ST772 (n = 340). Only  
 283 one representative isolate from longitudinal sampling of a single healthcare worker(n = 39) is  
 284 included (circle). **(b)** Average pairwise nucleotide diversity per site ( $\pi$ ), measured by region  
 285 (Australasia: orange, n = 36; Europe: blue, n = 244; South Asia: purple, n = 52). Error bars indicate  
 286 95% confidence intervals using non-parametric bootstrapping. Isolates from the Arabian Peninsula  
 287 (n = 2) and Hong Kong (n = 6) were excluded from the diversity analysis due to the small number of  
 288 samples from these regions. **(c)** Phylogenetic time-tree with the timescale estimated in Least Squares  
 289 Dating (LSD). The annotations for nodes represent the time of origin (in years) of basal strains and  
 290 subgroups A1, A2, A3. Times to the most recent common ancestor (TMRCA) for these lineages are  
 291 shown. Tips are colored according to the subgroup as per Figure 1a. The position of the root was  
 292 optimised during the analysis. Arrows indicate acquisition of three critical mobile genetic elements:  
 293 the PVL/*sea*-prophage  $\phi$ -IND772, an integrated multidrug resistance plasmid and the short  
 294 staphylococcal cassette chromosome *SCCmec*-V (5C2). **(d)** Times to the most recent common  
 295 ancestor of sub-groups in ST772 after removing recombination. Horizontal bars indicate 95%  
 296 confidence intervals for nodes (CI) using parametric bootstrapping in LSD.

297

298 **Figure 3:** Resistome and predicted resistance phenotypes across ST772. **(a)** Resistome mapped to

maximum likelihood phylogeny of ST772. Predicted resistant phenotype is depicted in red, while susceptible phenotype is depicted in blue. Presence of acquired resistance genes and mutations responsible for phenotype predictions are shown in red, while absence of these determinants is shown in gray. **(b)** Percent of isolates predicted resistant (gray) or susceptible (white) for all antimicrobials included in Mykrobe predictor **(c)** BLAST comparison of the multidrug-resistance plasmid in DAR4145 (middle) with the extrachromosomal plasmid 11809-p03 (top) and the SCC*mec*-IV integrated plasmid in ST80 (bottom), showing alignments > 1000 bp and > 95% nucleotide identity. The comparison highlights three regions harboring resistance genes (dark blue) and their regulators (light blue), which are flanked by transposition elements (green) and appear to have integrated with reversions and rearrangements into ST80 and ST772. Resistance genes include the  $\beta$ -lactam *blaZ* complex, aminoglycoside cluster *aphA3-sat4-aadE* and bacitracin resistance loci *bcrA/B*, as well as macrolide efflux genes *msrA* and *mphC*. Hypothetical proteins and genes of other annotated function are shown in white and dark gray, respectively. **(d)** Proportion of isolates predicted resistant to common antibiotics for basal isolates (white, n = 11) and isolates from ST772-A (gray, n = 291). Values above bars denote statistically significant differences between groups using Fisher's exact test where  $p < 0.01$ .

**Figure 4:** Phenotypic assays for representative strains from the basal group (white, n = 5) and ST772-A (gray, n = 10) for **(a)** optical density measurements (595 nm) of biofilm formation, accounting for day to day variability relative to control strain E-MRSA15 (%), **(b)** overnight growth in tryptic soy broth (doubling time per minute) measured by optical density (600 nm), **(c)** cytotoxicity of neat (100%) and diluted (30%) bacterial supernatant to THP-1 cells measured as cell death by flow cytometry, **(d)** absorbance measurements (404 nm) of erythrocyte haemolysis in neat (100%) and diluted (30%) bacterial supernatant, **(e)** lipase activity of *para*-nitrophenyl butyrate (pNPB) or *para*-nitrophenyl palmitate (pNPP) (release of pNP per minute) in neat bacterial supernatant measured by absorbance (410 nm). Slow growing strains H104580604 and HPAS101177P were considered outliers and removed from the boxplot for clarity after calculation of median and interquartile ranges and assessment of significance. Error bars show standard error; the asterisk denotes a significant difference in pNPP release (Welch's two-sided t-test,  $t = 3.4441$ ,  $df = 6.0004$ ,  $p = 0.0137$ ) between basal strains and ST772.

## Methods

### *Isolates*

Isolates were obtained from Australia (21), Bangladesh (3), Denmark (70), England (103), Germany (16), Hong Kong (6), India (44), Ireland (28), Italy (2), Netherlands (4), New Zealand (17), Norway (3), Saudi Arabia (1), Scotland (29) and the United Arab Emirates (1) between 2004 and 2012 (Supplementary Table 2). The collection was supplemented with six previously published genome sequences from India<sup>22,43,44</sup>. Notable samples include the initial isolates from Bangladesh and India<sup>10,11</sup>, two hospital-associated (NICU) clusters from Ireland<sup>20</sup> and longitudinal isolates from a single healthcare worker at a veterinary clinic sampled over two consecutive weeks (VET)<sup>45</sup>. Geographic regions were designated as Australasia (Australia, New Zealand), East Asia (Hong Kong), South Asia (India, Bangladesh), Arabian Peninsula (Saudi Arabia, United Arab Emirates) and Europe (Denmark, England, Germany, Ireland, Italy, Netherlands, Norway and Scotland).

### *Clinical data and epidemiology*

Anonymised patient data was obtained for the date of collection, clinical symptoms, geographic location, epidemiological connections based on family or travel-history, and acquisition in nosocomial- or community-environments, where available (Supplementary Table 2). Clinical symptoms were summarized as SSTI (abscesses, boils, ulcers, exudates, pus, ear and eye infections), urogenital- (vaginal swabs, urine), bloodstream- (bacteremia) or respiratory-infections (pneumonia, lungs abscesses) and colonization (swabs from ear, nose, throat, perineum or environmental) (Supplementary Table 2, Supplementary Figure 9). Literature and sample maps (Supplementary Maps 1 and 2) were constructed with *geonet*, a wrapper for geographic projections with Leaflet in R (<https://github.com/esteinig/geonet>).

Where available, acquisition in community- or healthcare-environments was recorded in accordance with guidelines from the CDC. Community-associated MRSA is therein classified as an infection in a person who has none of the following established risk factors for MRSA infection: isolation of MRSA more than 48 h after hospital admission; history of hospitalization, surgery, dialysis or residence in a long-term care facility within one year of the MRSA culture date; the presence of an indwelling catheter or a percutaneous device at the time of culture; or previous isolation of MRSA<sup>46,47</sup> (Supplementary Figure 9).

A valid epidemiological link to South Asia was declared if either travel- or family-background could be reliably traced to Bangladesh, India, Nepal or Pakistan. If both categories (travel and family) were unknown or one did not show a link to the region, we conservatively declared the link as unknown or absent, respectively. The longitudinal collection (n = 39) from a staff member at a veterinary hospital in England was treated as a single patient sample.

# *Sequencing, quality control and assembly*

Unique index-tagged libraries were created for each isolate, and multiplexed libraries were sequenced on the Illumina HiSeq with 100 bp paired-end reads. Read quality control was conducted with Trimmomatic<sup>48</sup>, Kraken<sup>49</sup> and FastQC (<https://www.bioinformatics.babraham.ac.uk/projects/fastqc>). Quality control identified a large proportion of reads classified as *Enterococcus faecalis* in sample HWM2178 (Supplementary Table 3). *In silico* micro-array typing (see below) identified an additional 13 isolates with possible intra-specific contamination due to simultaneous presence of *agr I* and *II*, as well as capsule types 5 and 8 (Supplementary Table 2). We excluded these isolates from all genomic analyses. Raw Illumina data were sub-sampled to 100x coverage and assembled with the SPAdes<sup>50</sup> pipeline Shovill (<https://github.com/tseemann/shovill>), which wraps SPAdes, Lighter<sup>51</sup>, FLASH<sup>52</sup>, BWA MEM<sup>53</sup>, SAMtools<sup>54</sup>, KMC<sup>55</sup> and Pilon<sup>56</sup>. Final assemblies were annotated with Prokka v1.11<sup>57</sup>. Samples from the veterinary staff member were processed and sequenced as described by Paterson et al.<sup>45</sup>.

# *MLST and SCC typing*

*In silico* multi-locus sequence typing (MLST) was conducted using mlst (<https://github.com/tseemann/mlst>) on the assembled genomes with the *S. aureus* database from PubMLST (<https://pubmlst.org/saureus/>). Three single locus variants (SLVs) of ST772 were detected and retained for the analysis, describing sequence types ST1573, ST3362 and ST3857 (Supplementary Table 2). Sequences of experimentally verified sets of probes for SCC- related and other *S. aureus* specific markers<sup>58,59</sup> were blasted against SPAdes assemblies (*in silico* micro-array typing), allowing prediction of presence or absence of these markers and detailed typing of SCC elements. We assigned MRSA to four isolates that failed precise SCC classification based on presence of *mecA* on the probe array and detection of the gene with Mykrobe predictor<sup>60</sup>.

## 396 *Variant calling*

397

398 Samples passing quality control (n = 340) were aligned to the PacBio reference genome DAR4145  
399 from Mumbai and variants were called with the pipeline Snippy (available at  
400 <https://github.com/tseemann/snippy>) which wraps BWA MEM, SAMtools, SnpEff<sup>61</sup> and  
401 Freebayes<sup>62</sup>. Core SNPs (n = 7,063) were extracted with *snippy-core* at default settings. We assigned  
402 canonical SNPs for ST772-A, as those present exclusively in all isolates of ST772-A, but not in the  
403 basal strains. Annotations of variants were based on the reference genome DAR4145.

404

## 405 *Phylogenetics and recombination*

406

407 A maximum-likelihood (ML) tree under the General Time Reversible model of nucleotide  
408 substitution with among-site rate heterogeneity across 4 categories (GTR +  $\Gamma$ ), ascertainment bias  
409 correction (Lewis) and 100 bootstrap (BS) replicates was generated based on 7,063 variant sites (core-  
410 genome SNPs) in RaxML-NG 0.5.0 (available at <https://github.com/amkozlov/raxml-ng>), which  
411 implements the core functionality of RAXML<sup>63</sup>. The tree with the highest likelihood out of ten  
412 replicates was midpoint-rooted and visualized with interactive Tree of Life (ITOL) (Figure 1a, 2a,  
413 Supplementary Figure 6, 12a)<sup>64</sup>. In all phylogenies (Figures 1a, 2a, 3a, Supplementary Figures 6, 10,  
414 12a) samples from the veterinary staff member were collapsed for clarity.

415

416 A confirmation alignment (n = 351) was computed as described above for resolving the pattern of  
417 divergence in the basal strains of ST772. The alignment included the CC1 strain MW2 as outgroup,  
418 as well as another known SLV of CC1, sequence type 573 (n = 10). The resulting subset of core SNPs  
419 (n = 25,701) was used to construct a ML phylogeny with RaxML-NG (GTR +  $\Gamma$ ) and 100 bootstrap  
420 replicates (Supplementary Figure 1). We also confirmed the general topology of our main phylogeny  
421 as described above using the whole genome alignment of 2,545,215 nucleotides generated by Snippy,  
422 masking sites if they contained missing (-) or uncertain (N) characters across ST772 (not shown).

423

424 Gubbins<sup>65</sup> was run on a complete reference alignment with all variant sites defined by Snippy to  
425 detect homologous recombination events, using a maximum of five iterations and the GTR +  $\Gamma$  model  
426 in RaxML (Supplementary Figure 10). A total of 205 segments were identified as recombinant  
427 producing a core alignment of 7,928 SNPs. Phylogenies were visualized using ITOL, *ape*<sup>66</sup>,  
428 *phytools*<sup>67</sup>, *ggtree*<sup>68</sup> or *plotTree* (<https://github.com/holtlab/plotTree/>). Patristic distances to the root  
429 of the phylogeny (Supplementary Figure 2) were computed in the *adephylo*<sup>69</sup> function *distRoot*.

430



# 431 *Dating analysis*

432

433 We used LSD v0.3<sup>70</sup> to obtain a time-scaled phylogenetic tree. This method fits a strict molecular  
434 clock to the data using a least-squares approach. Importantly, LSD does not explicitly model rate  
435 variation among lineages and it does not directly account for phylogenetic uncertainty. However, its  
436 accuracy is similar to that obtained using more sophisticated Bayesian approaches<sup>71</sup>, with the  
437 advantage of being computationally less demanding.

438

439 LSD typically requires a phylogenetic tree with branch lengths in substitutions per site, and  
440 calibrating information for internal nodes or for the tips of the tree. We used the phylogenetic tree  
441 inferred using Maximum likelihood in PhyML<sup>72</sup> (before and after removing recombination with  
442 Gubbins, as described above) using the GTR+ $\Gamma$  substitution model with 4 categories for the  $\Gamma$   
443 distribution. We used a combination of nearest-neighbour interchange and subtree-prune-regraft to  
444 search tree space. Because PhyML uses a stochastic algorithm, we repeated the analyses 10 times  
445 and selected that with the highest phylogenetic likelihood. To calibrate the molecular clock in LSD,  
446 we used the collection dates of the samples (i.e. heterochronous data). The position of the root can  
447 be specified *a priori*, using an outgroup or by optimising over all branches. We chose the latter  
448 approach. To obtain uncertainty around node ages and evolutionary rates we used the parametric  
449 bootstrap approach with 100 replicates implemented in LSD.

450

451 An important aspect of analysing heterochronous data is that the reliability of estimates of  
452 evolutionary rates and timescales is contingent on whether the data have temporal structure. In  
453 particular, a sufficient amount of genetic change should have accumulated over the sampling time.  
454 We investigated the temporal structure of the data by conducting a regression of the root-to-tip  
455 distances of the Maximum likelihood tree as a function of sampling time<sup>73</sup>, and a date-  
456 randomisation test<sup>74</sup>. Under the regression method, the slope of the line is a crude estimate of the  
457 evolutionary rate, and the extent to which the points deviate from the regression line determines the  
458 degree of clocklike behaviour, typically measured using the  $R^2$ <sup>75</sup>. The date randomisation test  
459 consists in randomising the sampling times of the sequences and re-estimating the rate each time.  
460 The randomisations correspond to the distribution of rate estimates under no temporal structure. As  
461 such, the data have strong temporal structure if the rate estimate using the correct sampling times is  
462 not within the range of those obtained from the randomisations<sup>76</sup>. We conducted 100  
463 randomisations, which suggested strong temporal structure for our data (Supplementary Figure 3).  
464 We also verified that the data did not display phylogenetic-temporal clustering, a pattern which  
465 sometimes misleads the date-randomisation test<sup>77</sup>.

466

467 Results from this analysis (substitution rates, and node age estimates) using phylogenies before and  
468 after removing recombination were nearly identical (Supplementary Figure 4, 5). We therefore  
469 chose to present results from our analysis after removing recombination.

470

# 471 *Nucleotide diversity*

472

473 Pairwise nucleotide diversity and SNP distance distributions for each region with  $n > 10$  (Australasia,  
474 Europe, South Asia) were calculated as outlined by Stucki et al.<sup>78</sup>. Pairwise SNP distances were  
475 computed using the SNP alignment from Snippy ( $n = 7,063$ ) and the *dist.dna* function from *ape* with  
476 raw counts and deletion of missing sites in a pairwise fashion. An estimate of average pairwise  
477 nucleotide diversity per site ( $\pi$ ) within each geographic region was calculated from the SNP  
478 alignments using raw counts divided by the alignment length. Confidence intervals for each region  
479 were estimated using 1000 bootstrap replicates across nucleotide sites in the original alignment via  
480 the *sample* function (with replacement) and 2.5% - 97.5% quantile range (Figure 2b).

481

# 482 *Population structure*

483

484 We used the network-analysis and -visualization tool NetView<sup>79,80</sup> (available at  
485 <http://github.com/esteinig/netview>) to delineate population subgroups in ST772. Pairwise Hamming  
486 distances were computed from the core SNP alignment derived from Snippy. The distance matrix  
487 was used to construct mutual k-nearest-neighbour networks from  $k = 1$  to  $k = 100$ . We ran three  
488 commonly used community detection algorithms as implemented in *igraph* to limit the parameter  
489 choice to an appropriate range for detecting fine-scale population structure: fast-greedy modularity  
490 optimization<sup>81</sup>, Infomap<sup>82</sup> and Walktrap<sup>83</sup>. We thereby accounted for differences in the mode of  
491 operation and resolution of algorithms. Plotting the number of detected communities against  $k$ , we  
492 were able to select a parameter value at which the results from the community detection were  
493 approximately congruent (Supplementary Figure 11).

494

495 Since we were interested in the large-scale population structure of ST772, we selected  $k = 40$  and  
496 used the low-resolution fast-greedy modularity optimisation to delineate final population subgroups.  
497 Community assignments were mapped back to the ML phylogeny of ST772 (Figure 1a). All  
498 subgroups agreed with the phylogenetic tree structure and were supported by  $\geq 99\%$  bootstrap values  
499 (Supplementary Figure 12). One exception was isolate HW\_M2760 located within ST772-A2 by  
500 phylogenetic analysis, but assigned to ST772-A3 by network analysis (Supplementary Figures 11,

12). This appeared to be an artefact of the algorithm, as its location and connectivity in the network representation matched its phylogenetic position within ST772-A2. The network and communities were visualized using the Fruchterman-Reingold algorithm (Figure 1c), excluding samples from the veterinary staff member in Figure 1c (Supplementary Figure 11).

### *Local transmission clusters*

We obtained approximate transmission clusters by employing a network approach supplemented with the ML topology and patient data, including date of collection, location of collection and patient family links and travel or family links to South Asia. We used pairwise SNP distances to define a threshold of 4 SNPs, corresponding to the maximum possible SNP distance obtained within one year under a core genome substitution rate of  $1.61 \times 10^{-6}$  nucleotide substitutions/site/year. We then constructed the adjacency matrix for a graph, in which isolates were connected by an undirected edge, if they had a distance of less or equal to 4 SNPs. All other isolates were removed from the graph and we mapped the resulting connected components to the ML phylogeny, showing that in each case the clusters were also reconstructed in the phylogeny, where isolates diverged from a recent common ancestor (gray highlights, Supplementary Figure 6). We then traced the identity of the connected components in the patient meta-data and added this information to each cluster. NICU clusters were reconstructed under these conditions.

### *Antimicrobial resistance, virulence factors and pan-genome*

Mykrobe predictor was employed for antibiotic susceptibility prediction and detection of associated resistance determinants and mutations. Mykrobe predictor has demonstrated sensitivity and specificity > 99% for predicting phenotypic resistance and is comparable to gold-standard phenotyping in *S. aureus*<sup>60</sup>. Predicted phenotypes were therefore taken as a strong indication for actual resistance phenotypes in ST772. Genotype predictions also reflect multidrug resistance profiles (aminoglycosides,  $\beta$ -lactams, fluoroquinolones, MLS, trimethoprim) reported for this clone in the literature<sup>16–18,20,84,85</sup>. As most resistance-associated MGEs in the complete reference genome DAR4145 are mosaic-like and flanked by repetitive elements<sup>18</sup>, we used specific diagnostic genes present as complete single copies in the reference annotation of DAR4145<sup>18</sup> to define presence of the IRP (*msrA*) and Tn4001 (*aacA-aphD*). Mykrobe predictor simultaneously called the *grrA* mutations S80F and S80Y for quinolone resistant phenotypes. However, in all cases one of the variants was covered at extremely low median k-mer depth (< 20) and we consequently assigned the variant with higher median k-mer depth at *grrA* (Supplementary Table 6).

536

537 ARIBA<sup>86</sup> with default settings and the core Virulence Factor database were used to detect the  
538 complement of virulence factors in ST772. We corroborated and extended our results with detailed  
539 *in-silico* microarray typing, including the presence of the *egc* gene cluster or *S. aureus* specific  
540 virulence factors such as the enterotoxin homologue ORF CM14. Differences in detection of relevant  
541 virulence factors between the *in silico* typing and ARIBA included, amongst others, *lukS/F-PVL* (337  
542 vs. 336), *sea* carried on the  $\phi$ -IND772 prophage (336 vs. 326), *sec* (333 vs 328) and *sak* (1 vs. 2).  
543 Since *in silico* microarray typing was based on assembled genomes and may therefore be prone to  
544 assembly errors, we used results from the read-based typing with ARIBA to assess statistical  
545 significance of virulence factors present in basal strains and ST772-A (Supplementary Figure 7).

546

547 Pan-genome analysis was conducted using Prokka annotated assemblies in Roary<sup>87</sup>, with minimum  
548 protein BLAST identity at 95% and minimum percentage for a gene to be considered core at 99%  
549 (Supplementary Figure 13). A gene synteny comparison between major SCCmec types was plotted  
550 with genoPlotR<sup>88</sup> (Supplementary Figure 8). A nucleotide BLAST comparison between the  
551 extrachromosomal plasmid 11809-03 of USA300, the integrated resistance plasmid in the ST772  
552 reference genome DAR4145 and the integrated plasmid region in strain 11819-07 of ST80 was  
553 plotted with geneD3 (<https://github.com/esteinig/geneD3/>), showing segments > 1kb (Supplementary  
554 File 1).

555

556 We searched for the three resistance regions which aligned to the 11819-07 and the 11809-03 plasmid  
557 (DAR4145 reference genome; R1: 1456024-1459959 bp, R2: 1443096-1448589 bp and R3:  
558 1449679-1453291 bp) in all completed *S. aureus* genomes (including plasmids) in RefSeq (NCBI)  
559 and the NCTC3000 project (<http://www.sanger.ac.uk/resources/downloads/bacteria/nctc/>) using  
560 nctc-tools (<https://github.com/esteinig/nctc-tools>) and nucleotide BLAST with a minimum of 90%  
561 coverage and identity (n = 273). Since the IRP is mosaic-like and composed of several mobile regions,  
562 we only retained query results, if all three of the regions were detected (Supplementary Table 9). We  
563 then traced the integration sites in the accessions, determining whether integrations occurred the  
564 chromosome or plasmids. Multi-locus sequence types were assigned using *mlst*  
565 (<https://github.com/tseemann/mlst>).

566

## 567 *Growth curves*

568

569 *S. aureus* strains were grown overnight in 5 mL tryptic soy broth (TSB, Fluka) with shaking (180  
570 rpm) at 37 °C. Overnight cultures were diluted 1:1000 in fresh TSB and 200  $\mu$ L was added to a 96 –

well plate (Costar) in triplicate. Growth was measured 37 °C, with shaking (300 rpm) using a FLUORostar fluorimeter (BMG Labtech) using an absorbance wavelength of 600 nm. Growth curves represent the mean of triplicate results.

#### Cell culture conditions

The monocyte-macrophage THP-1 cell line was maintained in suspension in 30 mL Roswell Park Memorial Medium Institute (RPMI-1640) medium, supplemented with 10% heat-inactivated fetal bovine serum (FBS), 1 µM L-glutamine, 200 units/mL penicillin, and 0.1 mg/mL streptomycin at 37 °C in a humidified incubator with 5% CO<sub>2</sub>. Cells were harvested by centrifugation at 700 x g for 10 min at room temperature and re-suspended to a final density of 1–1.2 x 10<sup>6</sup> cells/mL in tissue-grade phosphate buffered saline, typically yielding >95 % viable cells as determined by easyCyte flow cytometry (Millipore).

Human erythrocytes were harvested from 10 mL of human blood following treatment in sodium heparin tubes (BD). Whole blood was centrifuged at 500 x g for 10 min at 4 °C. Supernatant (plasma) was aspirated and cells were washed twice in 0.9 % NaCl and centrifuged at 700 x g for 10 min. Cell pellet was gently re-suspended in 0.9 % NaCl and diluted to 1 % (v/v).

#### Cytotoxicity assay

To monitor *S. aureus* toxicity, *S. aureus* strains were grown overnight in TSB, diluted 1:1000 in 5 mL fresh TSB and grown for 18 h at 37 °C with shaking (180 rpm). Bacterial supernatants were prepared by centrifugation of 1 mL of bacterial culture at 20,000 x g for 10 min. For assessing toxicity to THP-1 cells, 20 µL of cells were incubated with 20 µL of bacterial supernatant and incubated for 12 min at 37 °C. Both neat and 30% diluted supernatant (in TSB) were used as certain *S. aureus* strains were considerably more toxic than others. Cell death was quantified using easyCyte flow cytometry using the Guava viability stain according to manufacturer's instructions. Experiments were done in triplicate. For assessing haemolysis, 150 µL of 1% (v/v) erythrocytes were incubated with 50 µL of either neat and 30% supernatant in a 96 well plate for 30 min at 37°C. Plates were centrifuged for 5 min at 300 x g and 75 µL of supernatant was transferred to a new plate and absorbance was measured at 404nm using a FLUORostar fluorimeter (BMG Labtech). Normalised fluorescence was achieved using the equation  $(A_t - A_0) / (A_m - A_0)$  where  $A_t$  is the haemolysis absorbance value of a strain,  $A_0$  is the minimum absorbance value (negative control of 0.9% NaCl) and  $A_m$  is the maximum absorbance value (positive control of 1 % triton X-100).

## 606 *Lipase assay*

607

608 Bacterial supernatants used in the above cytotoxicity assays were also used to assess lipase activity,  
 609 using the protocol published by Cadieux *et al.*<sup>89</sup> with modifications. Briefly, 8mM *para*-nitrophenyl  
 610 butyrate (pNPB), the short chain substrate, or *para*-nitrophenyl palmitate (pNPP), the long chain  
 611 substrate, (Sigma) was mixed with a buffer (50mM Tris-HCl (pH 8.0), 1mg/ml gum Arabic and  
 612 0.005% Triton-X100) in a 1:9 ratio to create assay mixes. A standard curve using these assay mixes  
 613 and *para*-nitrophenyl (pNP) (Sigma) was created, and 200µl of each dilution was pipetted into one  
 614 well of a 96-well plate (Costar). 180µl of the assay mixes was pipetted into the remaining wells of a  
 615 96-well plate, and 20µl of the harvested bacterial supernatant was mixed into the wells. The plate was  
 616 placed in a FLUOstar Omega microplate reader (BMG Labtech) at 37°C, and a reading at 410nm was  
 617 taken every 5 min.s for 1h. The absorbance readings were converted to µM pNP released/min. using  
 618 the standard curve.

619

## 620 *Biofilm formation*

621

622 Semi-quantitative measurements of biofilm formation on 96-well, round-bottom, polystyrene plates  
 623 (Costar) was determined based on the classical, crystal violet method of Ziebuhr *et al.*<sup>90</sup>. 18 h bacterial  
 624 cultures grown in TSB were diluted 1:40 into 100 µL TSB containing 0.5 % glucose. Perimeter wells  
 625 of the 96-well plate were filled with sterile H<sub>2</sub>O and plates were placed in a separate plastic container  
 626 inside a 37°C incubator and grown for 24 h under static conditions. Following 24 h growth, plates  
 627 were washed five times in PBS, dried and stained with 150 µL of 1% crystal violet for 30 min at room  
 628 temperature. Following five washes of PBS, wells were re-suspended in 200 µL of 7% acetic acid,  
 629 and optical density at 595 nm was measured using a FLUOROstar fluorimeter (BMG Labtech). To  
 630 control for day to day variability, a control strain (E-MRSA15) was included on each plate in  
 631 triplicate, and absorbance values were normalised against this. Experiments were done using six  
 632 technical repeats from 2 different experiments.

633

## 634 *Statistical analysis*

635

636 All statistical analyses were carried out in R or python and considered significant at  $p < 0.05$ , except  
 637 for comparisons of proportions across the multiple virulence and resistance elements, which we  
 638 considered be statistically significant at  $p < 0.01$ . Veterinary samples ( $n = 39$ ) were restricted to one  
 639 isolate (one patient, Staff\_E1A) for statistical comparison of region of isolation, proportion of  
 640 resistance, virulence and MSSA between basal strains and ST772-A ( $n = 302$ , Main, Figures 3d,



Supplementary Figure 7). Differences in pairwise SNP distance and nucleotide diversity between all regions were assessed using non-parametric Kruskal-Wallis test and post-hoc Dunn's test for multiple comparisons with Bonferroni correction, as distributions were assumed to be not normally distributed (Figure 2b, n = 340, Supplementary Figure 2). Phenotypic differences were assessed for normality with Shapiro-Wilk tests. We consequently used either Welch's two-sided t-test or the non-parametric two-sided Wilcoxon rank-sum test (Figure 4, Supplementary Table 8).

# *Code availability*

Core analyses, including parameter settings, cluster resource configurations and versioned software distributions are reproducible through the *bengal-bay-0.1* workflow, which can be found along with other scripts and data files at our GitHub repository (<https://github.com/esteinig/ST772>) and can be executed with PathFinder (<https://github.com/esteinig/pathfinder>). The workflow implements Anaconda virtual environments, including software distributed in the Bioconda<sup>91</sup> channel and is implemented in Snakemake<sup>92</sup>. Analyses were conducted on the Cheetah cluster at Menzies School of Health Research, Darwin.

# *Data availability*

Short-read sequences have been deposited at ENA under accession numbers detailed in Supplementary Table 2. Additional isolates from India are available from the SRA under accession numbers SRR404118, SRR653209, SRR653212 and SRR747869-SRR747873. Outgroup strains used in the context phylogeny are available from ENA under accession numbers SRR592258 (MW2), ERR217298, ERR217349, ERR221806, ERR266712, ERR279022, ERR279023, ERR278908, ERR279026, ERR716976, ERR717011 (ST573). The ST772 reference genome DAR4145 is available at GenBank under accession number CP010526.1.

# *Author contributions*

EJS, ST conducted the bioinformatics analysis; SD performed the dating analysis; SM, PS, PA performed *in silico* typing and provided bioinformatics support; DS provided support on the computing cluster; MY, ML, RM conducted phenotyping experiments; DAR, DW, AK, RG, ED, RE, SM, MI, MO, GC, AP, GB, AS, DC, AP, AM, HdL, HW, NK, HH, BS, FL, SP, SW, HA, LS, SH provided strains and relevant meta-data; EJS, ST, DAR, SM, MTGH wrote the manuscript; all authors contributed to critical review of the manuscript. ST directed the project with support from SB and JP.

676

677 *Acknowledgements*

678

679 We thank the library construction, sequencing, and core informatics teams at the Wellcome Trust  
 680 Sanger Institute. We also extend our gratitude to Anand Manoharan for comments on the manuscript  
 681 and strains from India. ST is supported by an Australian National Health and Medical Research  
 682 Council Career Development Award (#1145033). DAR is supported by NIH grant GM080602. DC  
 683 and AS are supported by an Irish Health Research Board grant HRA-POR-2015-1051. MO is  
 684 supported by an NHMRC project grant (#1065908).

685

686 *Competing financial interests*

687

688 There are no competing financial interests to declare.

689

690 *Materials and correspondence*

691

692 Steven Y.C. Tong

## References

1. Tong, S. Y. C. & Kearns, A. M. Community-associated MRSA from the Indian subcontinent. *Lancet Infect. Dis.* **13**, 734–735 (2013).
2. Earls, M. R. *et al.* The recent emergence in hospitals of multidrug-resistant community-associated sequence type 1 and spa type t127 methicillin-resistant *Staphylococcus aureus* investigated by whole-genome sequencing: Implications for screening. *PLoS One* **12**, e0175542 (2017).
3. Wang, L. *et al.* Multidrug-resistant clones of community-associated methicillin-resistant *Staphylococcus aureus* isolated from Chinese children and the resistance genes to clindamycin and mupirocin. *J. Med. Microbiol.* **61**, 1240–1247 (2012).
4. Lee, G. C. *et al.* Emerging multidrug resistance in community-associated *Staphylococcus aureus* involved in skin and soft tissue infections and nasal colonization. *J. Antimicrob. Chemother.* **72**, 2461–2468 (2017).
5. Diekema, D. J. *et al.* Continued Emergence of USA300 Methicillin-Resistant *Staphylococcus aureus* in the United States: Results from a Nationwide Surveillance Study. *Infect. Control Hosp. Epidemiol.* **35**, 285–292 (2014).
6. Ward, M. J. *et al.* Identification of source and sink populations for the emergence and global spread of the East-Asia clone of community-associated MRSA. *Genome Biol.* **17**, 160 (2016).
7. Li, M. *et al.* Increased Community-Associated Infections Caused by Panton-Valentine Leukocidin–Negative MRSA, Shanghai, 2005–2014. *Emerg. Infect. Dis.* **22**, 1988–1991 (2016).
8. Tong, S. Y. C., Davis, J. S., Eichenberger, E., Holland, T. L. & Fowler, V. G. J. *Staphylococcus aureus* infections: epidemiology, pathophysiology, clinical manifestations, and management. *Clin. Microbiol. Rev.* **28**, 603–661 (2015).
9. Suaya, J. A. *et al.* Incidence and cost of hospitalizations associated with *Staphylococcus aureus* skin and soft tissue infections in the United States from 2001 through 2009. *BMC Infect. Dis.* **14**, 296 (2014).
10. Afroz, S. *et al.* Genetic characterization of *Staphylococcus aureus* isolates carrying Panton-Valentine leukocidin genes in Bangladesh. *Jpn. J. Infect. Dis.* **61**, 393–396 (2008).
11. Goering, R. V. *et al.* Molecular epidemiology of methicillin-resistant and methicillin-susceptible *Staphylococcus aureus* isolates from global clinical trials. *J. Clin. Microbiol.* **46**, 2842–2847 (2008).
12. Chen, C.-J. & Huang, Y.-C. New epidemiology of *Staphylococcus aureus* infection in Asia.

- 728 *Clin. Microbiol. Infect.* **20**, 605–623 (2014).
- 729 13. D’Souza, N., Rodrigues, C. & Mehta, A. Molecular characterization of methicillin-resistant  
730 *Staphylococcus aureus* with emergence of epidemic clones of sequence type (ST) 22 and ST  
731 772 in Mumbai, India. *J. Clin. Microbiol.* **48**, 1806–1811 (2010).
- 732 14. Nadig, S. *et al.* *Staphylococcus aureus* eye infections in two Indian hospitals: emergence of  
733 ST772 as a major clone. *Clin. Ophthalmol.* **6**, 165–173 (2012).
- 734 15. Manoharan, A. *et al.* An outbreak of post-partum breast abscesses in Mumbai, India caused  
735 by ST22-MRSA-IV: genetic characteristics and epidemiological implications. *Epidemiol.*  
736 *Infect.* **140**, 1809–1812 (2012).
- 737 16. Blomfeldt, A. *et al.* Emerging multidrug-resistant Bengal Bay clone ST772-MRSA-V in  
738 Norway: molecular epidemiology 2004–2014. *Eur. J. Clin. Microbiol. Infect. Dis.* **36**, 1911–  
739 1921 (2017).
- 740 17. Chakrakodi, B., Prabhakara, S., Nagaraj, S., Etienne, J. & Arakere, G. High Prevalence of  
741 ciprofloxacin resistance in community associated *Staphylococcus aureus* in a tertiary care  
742 Indian hospital. *Adv. Microbiol.* **4**, 133–141 (2014).
- 743 18. Steinig, E. J. *et al.* Single-molecule sequencing reveals the molecular basis of multidrug-  
744 resistance in ST772 methicillin-resistant *Staphylococcus aureus*. *BMC Genomics* **16**, 388  
745 (2015).
- 746 19. Ellington, M. J., Ganner, M., Warner, M., Cookson, B. D. & Kearns, A. M. Polyclonal  
747 multiply antibiotic-resistant methicillin-resistant *Staphylococcus aureus* with Panton-  
748 Valentine leucocidin in England. *J Antimicrob Chemother* **65**, 46–50 (2010).
- 749 20. Brennan, G. I. *et al.* Emergence of hospital- and community-associated Panton-Valentine  
750 leukocidin-positive methicillin-resistant *Staphylococcus aureus* genotype ST772-MRSA-V in  
751 Ireland and detailed investigation of an ST772-MRSA-V cluster in a neonatal intensive care  
752 unit. *J. Clin. Microbiol.* **50**, 841–847 (2012).
- 753 21. Prabhakara, S. *et al.* Genome sequencing unveils a novel sea enterotoxin-carrying PVL  
754 phage in *Staphylococcus aureus* ST772 from India. *PLoS One* **8**, e60013 (2013).
- 755 22. Balakuntla, J., Prabhakara, S. & Arakere, G. Novel rearrangements in the staphylococcal  
756 cassette chromosome mec type V elements of Indian ST772 and ST672 methicillin resistant  
757 *Staphylococcus aureus* strains. *PLoS One* **9**, e94293 (2014).
- 758 23. Schijffelen, M. J., Boel, C. H. E., van Strijp, J. A. G. & Fluit, A. C. Whole genome analysis  
759 of a livestock-associated methicillin-resistant *Staphylococcus aureus* ST398 isolate from a  
760 case of human endocarditis. *BMC Genomics* **11**, 376 (2010).
- 761 24. Kennedy, A. D. *et al.* Complete nucleotide sequence analysis of plasmids in strains of  
762 *Staphylococcus aureus* clone USA300 reveals a high level of identity among isolates with

- 763 closely related core genome sequences. *J. Clin. Microbiol.* **48**, 4504–4511 (2010).
- 764 25. Stegger, M. *et al.* Genome sequence of *Staphylococcus aureus* strain 11819-97, an ST80-IV  
765 European community-acquired methicillin-resistant isolate. *J. Bacteriol.* **194**, 1625–6 (2012).
- 766 26. Cheung, A. I., Projan, S. J., Edelstein, R. E. & Fischetti, V. A. Cloning, expression, and  
767 nucleotide sequence of a *Staphylococcus aureus* gene (fbpA) encoding a fibrinogen-binding  
768 protein. *Infect. Immun.* **63**, 1914–1920 (1995).
- 769 27. White, M. J., Boyd, J. M., Horswill, A. R. & Nauseef, W. M. Phosphatidylinositol-specific  
770 phospholipase C contributes to survival of *Staphylococcus aureus* USA300 in human blood  
771 and neutrophils. *Infect. Immun.* **82**, 1559–1571 (2014).
- 772 28. Truong-Bolduc, Q. C., Villet, R. A., Estabrooks, Z. A. & Hooper, D. C. Native efflux pumps  
773 contribute resistance to antimicrobials of skin and the ability of *Staphylococcus aureus* to  
774 colonize skin. *J. Infect. Dis.* **209**, 1485–1493 (2014).
- 775 29. Pokhrel, R. H. *et al.* Detection of ST772 Panton-Valentine leukocidin-positive methicillin-  
776 resistant *Staphylococcus aureus* (Bengal Bay clone) and ST22 *S. aureus* isolates with a  
777 genetic variant of elastin binding protein in Nepal. *New Microbes New Infect.* **11**, 20–27  
778 (2017).
- 779 30. Madzgalla, S. *et al.* Molecular characterization of *Staphylococcus aureus* isolates causing  
780 skin and soft tissue infections in patients from Malakand, Pakistan. *Eur. J. Clin. Microbiol.*  
781 *Infect. Dis.* **35**, 1541–1547 (2016).
- 782 31. Stegger, M. *et al.* Origin and evolution of European community-acquired methicillin-  
783 resistant *Staphylococcus aureus*. *MBio* **5**, e01044-14 (2014).
- 784 32. Planet, P. J. *et al.* Emergence of the epidemic methicillin-resistant *Staphylococcus aureus*  
785 strain USA300 coincides with horizontal transfer of the arginine Catabolic Mobile Element  
786 and speG-mediated Adaptations for Survival on Skin. *MBio* **4**, (2013).
- 787 33. Strauß, L. *et al.* Origin, evolution, and global transmission of community-acquired  
788 &lt;em>Staphylococcus aureus</em> ST8. *Proc. Natl. Acad. Sci.* **114**, E10596 LP-  
789 E10604 (2017).
- 790 34. Lee, S. M. *et al.* Fitness cost of staphylococcal cassette chromosome mec in methicillin-  
791 resistant *Staphylococcus aureus* by way of continuous culture. *Antimicrob. Agents*  
792 *Chemother.* **51**, 1497–1499 (2007).
- 793 35. Ender, M., McCallum, N., Adhikari, R. & Berger-Bächi, B. Fitness cost of SCCmec and  
794 methicillin resistance levels in *Staphylococcus aureus*. *Antimicrob. Agents Chemother.* **48**,  
795 2295–2297 (2004).
- 796 36. Collins, J. *et al.* Offsetting virulence and antibiotic resistance costs by MRSA. *ISME J* **4**,  
797 577–584 (2010).

- 798 37. Zanger, P. *et al.* Import and spread of Pantone-Valentine Leukocidin-positive *Staphylococcus*  
799 *aureus* through nasal carriage and skin infections in travelers returning from the tropics and  
800 subtropics. *Clin. Infect. Dis.* **54**, 483–492 (2012).
- 801 38. Planet, P. J. *et al.* Parallel epidemics of community-associated methicillin-resistant  
802 *Staphylococcus aureus* USA300 infection in North and South America. *J. Infect. Dis.* **212**,  
803 1874–82 (2015).
- 804 39. Nimmo, G. R. USA300 abroad: global spread of a virulent strain of community-associated  
805 methicillin-resistant *Staphylococcus aureus*. *Clin. Microbiol. Infect.* **18**, 725–734 (2012).
- 806 40. Holden, M. T. G. *et al.* A genomic portrait of the emergence, evolution, and global spread of  
807 a methicillin-resistant *Staphylococcus aureus* pandemic. *Genome Res.* **23**, 653–664 (2013).
- 808 41. Castillo-Ramírez, S. *et al.* Phylogeographic variation in recombination rates within a global  
809 clone of methicillin-resistant *Staphylococcus aureus*. *Genome Biol.* **13**, 126 (2012).
- 810 42. Harris, S. R. *et al.* Evolution of MRSA during hospital transmission and intercontinental  
811 spread. *Science* **327**, 469–474 (2010).
- 812 43. Prabhakara, S. *et al.* Draft genome sequence of *Staphylococcus aureus* 118 (ST772), a major  
813 disease clone from India. *J. Bacteriol.* **194**, 3727–3728 (2012).
- 814 44. Prabhakara, S. *et al.* Genome sequencing unveils a novel sea enterotoxin-carrying PVL  
815 phage in *Staphylococcus aureus* ST772 from India. *PLoS One* **8**, e60013 (2013).
- 816 45. Paterson, G. K. *et al.* Capturing the cloud of diversity reveals complexity and heterogeneity  
817 of MRSA carriage, infection and transmission. *Nat. Commun.* **6**, 6560 (2015).
- 818 46. Morrison, M. A., Hageman, J. C. & Kleven, R. M. Case definition for community-  
819 associated methicillin-resistant *Staphylococcus aureus*. *J. Hosp. Infect.* **62**, 241 (2006).
- 820 47. Fridkin, S. K. *et al.* Methicillin-resistant *Staphylococcus aureus* disease in three  
821 communities. *N. Engl. J. Med.* **352**, 1436–1444 (2005).
- 822 48. Bolger, A. M., Lohse, M. & Usadel, B. Trimmomatic: a flexible trimmer for Illumina  
823 sequence data. *Bioinformatics* **30**, 2114–2120 (2014).
- 824 49. Wood, D. E. & Salzberg, S. L. Kraken: ultrafast metagenomic sequence classification using  
825 exact alignments. *Genome Biol.* **15**, 1–12 (2014).
- 826 50. Bankevich, A. SPAdes: a new genome assembly algorithm and its applications to single-cell  
827 sequencing. *J Comput Biol* **19**, 455–477 (2012).
- 828 51. Song, L., Florea, L. & Langmead, B. Lighter: fast and memory-efficient sequencing error  
829 correction without counting. *Genome Biol.* **15**, 509 (2014).
- 830 52. Magoč, T. & Salzberg, S. L. FLASH: fast length adjustment of short reads to improve  
831 genome assemblies. *Bioinformatics* **27**, 2957–2963 (2011).
- 832 53. Li, H. Aligning sequence reads, clone sequences and assembly contigs with BWA-MEM.



833 *ArXiv* (2013).

834 54. Li, H. *et al.* The Sequence Alignment/Map format and SAMtools. *Bioinformatics* **25**, 2078–  
835 2079 (2009).

836 55. Deorowicz, S., Kokot, M., Grabowski, S. & Debudaj-Grabysz, A. KMC 2: fast and resource-  
837 frugal k-mer counting. *Bioinformatics* **31**, 1569–1576 (2015).

838 56. Walker, B. J. *et al.* Pilon: An Integrated Tool for Comprehensive Microbial Variant  
839 Detection and Genome Assembly Improvement. *PLoS One* **9**, e112963 (2014).

840 57. Seemann, T. Prokka: rapid prokaryotic genome annotation. *Bioinformatics* **30**, 2068–2069  
841 (2014).

842 58. Monecke, S. *et al.* A field guide to pandemic, epidemic and sporadic clones of methicillin-  
843 resistant *Staphylococcus aureus*. *PLoS One* **6**, e17936 (2011).

844 59. Monecke, S. *et al.* Diversity of SCCmec Elements in *Staphylococcus aureus* as Observed in  
845 South-Eastern Germany. *PLoS One* **11**, e0162654 (2016).

846 60. Bradley, P. *et al.* Rapid antibiotic-resistance predictions from genome sequence data for  
847 *Staphylococcus aureus* and *Mycobacterium tuberculosis*. *Nat. Commun.* **6**, 10063 (2015).

848 61. Cingolani, P. *et al.* A program for annotating and predicting the effects of single nucleotide  
849 polymorphisms, SnpEff: SNPs in the genome of *Drosophila melanogaster* strain w(1118);  
850 iso-2; iso-3. *Fly (Austin)*. **6**, 80–92 (2012).

851 62. Garrison, E. & Marth, G. Haplotype-based variant detection from short-read sequencing.  
852 *ArXiv* (2012).

853 63. Stamatakis, A. RAxML Version 8: a tool for phylogenetic analysis and post-analysis of large  
854 phylogenies. *Bioinformatics* **30**, 1312–1313 (2014).

855 64. Letunic, I. & Bork, P. Interactive Tree Of Life (iTOL): an online tool for phylogenetic tree  
856 display and annotation. *Bioinformatics* **23**, 127–128 (2007).

857 65. Croucher, N. J. *et al.* Rapid phylogenetic analysis of large samples of recombinant bacterial  
858 whole genome sequences using Gubbins. *Nucleic Acids Res.* **43**, 15 (2015).

859 66. Paradis, E., Claude, J. & Strimmer, K. APE: analyses of phylogenetics and evolution in R  
860 language. *Bioinformatics* **20**, 289–290 (2004).

861 67. Revell, L. J. phytools: an R package for phylogenetic comparative biology (and other things).  
862 *Methods Ecol. Evol.* **3**, 217–223 (2012).

863 68. Yu, G., Smith, D. K., Zhu, H., Guan, Y. & Lam, T. T.-Y. ggtree: an r package for  
864 visualization and annotation of phylogenetic trees with their covariates and other associated  
865 data. *Methods Ecol. Evol.* **8**, 28–36 (2017).

866 69. Jombart, T., Balloux, F. & Dray, S. adephylo: new tools for investigating the phylogenetic  
867 signal in biological traits. *Bioinformatics* **26**, 1907–1909 (2010).

- 868 70. To, T.-H., Jung, M., Lycett, S. & Gascuel, O. Fast dating using least-squares criteria and  
869 algorithms. *Syst. Biol.* **65**, 82–97 (2016).
- 870 71. Duchêne, S., Geoghegan, J. L., Holmes, E. C. & Ho, S. Y. W. Estimating evolutionary rates  
871 using time-structured data: a general comparison of phylogenetic methods. *Bioinformatics*  
872 **32**, 3375–3379 (2016).
- 873 72. Guindon, S. *et al.* New algorithms and methods to estimate maximum-likelihood  
874 phylogenies: assessing the performance of PhyML 3.0. *Syst Biol* **59**, 307–321 (2010).
- 875 73. Korber, B. *et al.* Timing the ancestor of the HIV-1 pandemic strains. *Science (80-. )*. **288**,  
876 1789–1796 (2000).
- 877 74. Ramsden, C., Holmes, E. C. & Charleston, M. A. Hantavirus evolution in relation to its  
878 rodent and insectivore hosts: no evidence for codivergence. *Mol. Biol. Evol.* **26**, 143–153  
879 (2009).
- 880 75. Rambaut, A., Lam, T. T., Max Carvalho, L. & Pybus, O. G. Exploring the temporal structure  
881 of heterochronous sequences using TempEst (formerly Path-O-Gen). *Virus Evol.* **2**, vew007  
882 (2016).
- 883 76. Duchêne, S., Duchêne, D., Holmes, E. C. & Ho, S. Y. W. The performance of the date-  
884 randomization test in phylogenetic analyses of time-structured virus data. *Mol. Biol. Evol.* **32**,  
885 1895–1906 (2015).
- 886 77. Murray, G. G. R. *et al.* The effect of genetic structure on molecular dating and tests for  
887 temporal signal. *Methods Ecol. Evol.* **7**, 80–89 (2016).
- 888 78. Stucki, D. *et al.* *Mycobacterium tuberculosis* lineage 4 comprises globally distributed and  
889 geographically restricted sublineages. *Nat Genet* **48**, 1535–1543 (2016).
- 890 79. Neuditschko, M., Khatkar, M. S. & Raadsma, H. W. NetView: a high-definition network-  
891 visualization approach to detect fine-scale population structures from genome-wide patterns  
892 of variation. *PLoS One* **7**, e48375 (2012).
- 893 80. Steinig, E. J., Neuditschko, M., Khatkar, M. S., Raadsma, H. W. & Zenger, K. R. NetView  
894 P : a network visualization tool to unravel complex population structure using genome-wide  
895 SNPs. *Mol. Ecol. Resour.* **16**, 216–227 (2016).
- 896 81. Girvan, M. & Newman, M. E. J. Community structure in social and biological networks.  
897 *Proc. Natl. Acad. Sci. U. S. A.* **99**, 7821–7826 (2002).
- 898 82. Rosvall, M. & Bergstrom, C. T. Maps of random walks on complex networks reveal  
899 community structure. *Proc. Natl. Acad. Sci. U. S. A.* **105**, 1118–1123 (2008).
- 900 83. Pons, P. & Latapy, M. Computing communities in large networks using random walks. *J.*  
901 *Graph Algorithms Appl.* **10**, 191–218 (2006).
- 902 84. Ellington, M. J., Ganner, M., Warner, M., Cookson, B. D. & Kearns, A. M. Polyclonal

903 multiply antibiotic-resistant methicillin-resistant *Staphylococcus aureus* with Panton-  
904 Valentine leucocidin in England. *J. Antimicrob. Chemother.* **65**, 46–50 (2010).

905 85. Shore, A. C. *et al.* Panton-Valentine leukocidin-positive *Staphylococcus aureus* in Ireland  
906 from 2002 to 2011: 21 clones, frequent importation of clones, temporal shifts of predominant  
907 methicillin-resistant *S. aureus* clones, and increasing multiresistance. *J. Clin. Microbiol.* **52**,  
908 859–870 (2014).

909 86. Hunt, M. *et al.* ARIBA: rapid antimicrobial resistance genotyping directly from sequencing  
910 reads. *Microb. Genomics* **3**, e000131 (2017).

911 87. Page, A. J. *et al.* Roary: rapid large-scale prokaryote pan genome analysis. *Bioinformatics*  
912 **31**, 3691–3693 (2015).

913 88. Guy, L., Roat Kultima, J. & Andersson, S. G. E. genoPlotR: comparative gene and genome  
914 visualization in R. *Bioinforma.* **26**, 2334–2335 (2010).

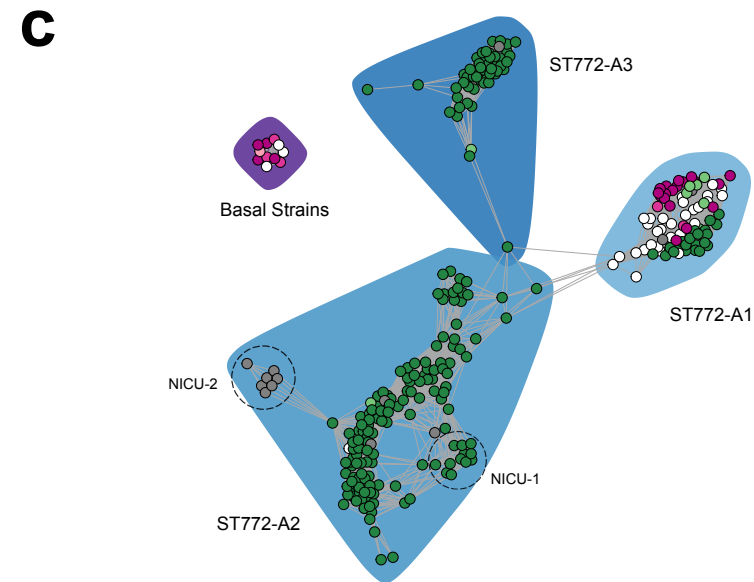
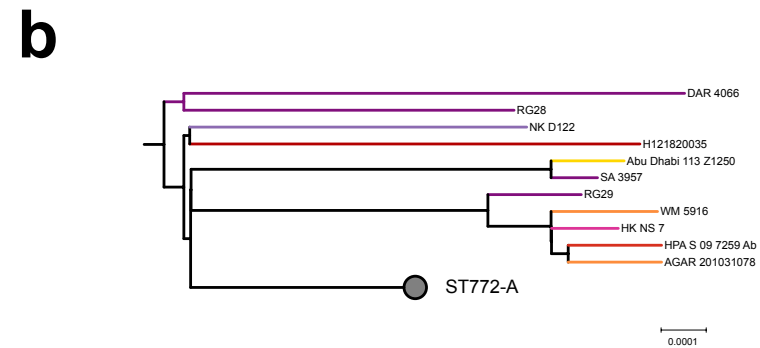
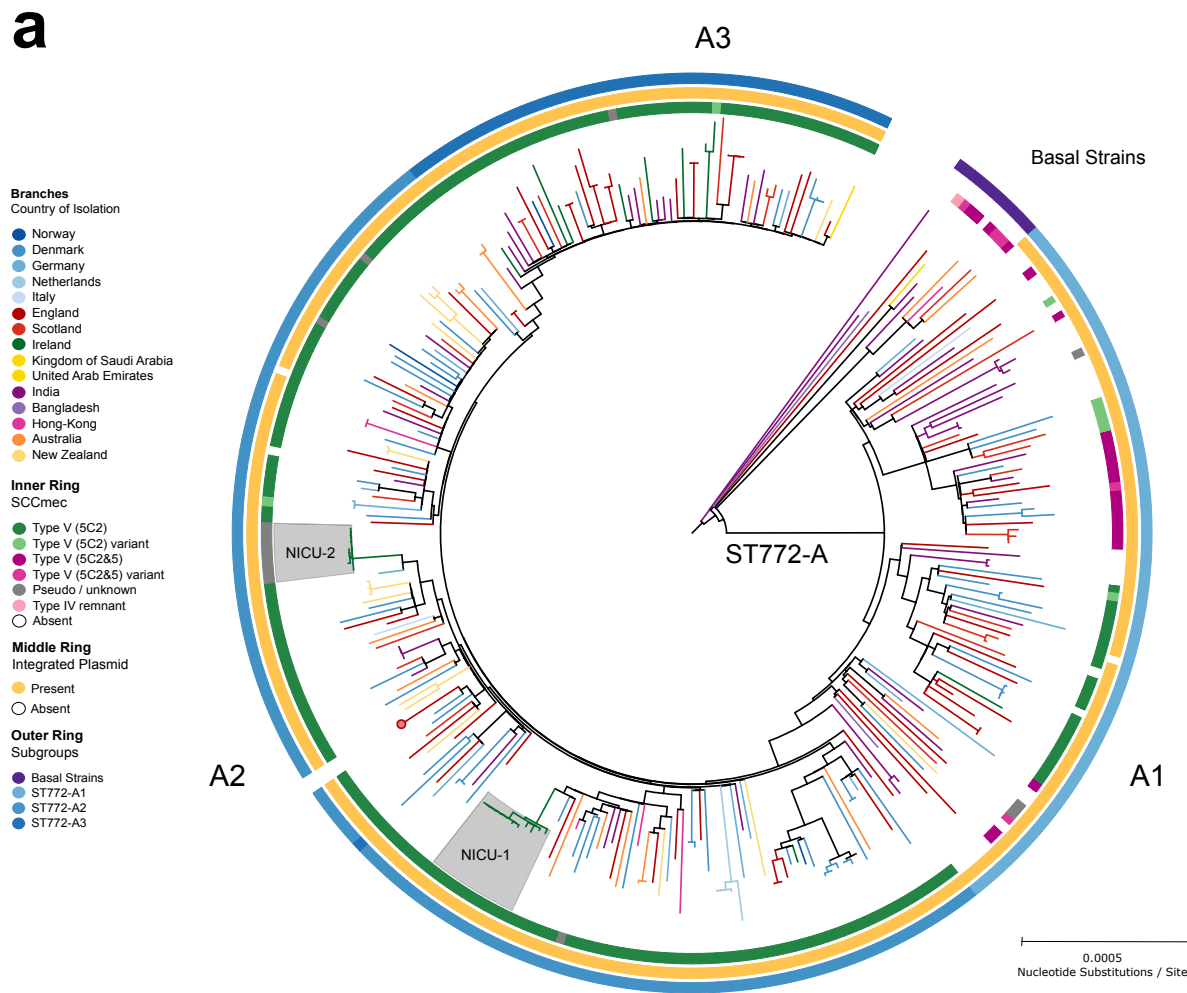
915 89. Cadieux, B., Vijayakumaran, V., Bernards, M. A., McGavin, M. J. & Heinrichs, D. E. Role  
916 of lipase from community-associated methicillin-resistant *Staphylococcus aureus* strain  
917 USA300 in hydrolyzing triglycerides into growth-inhibitory free fatty acids. *J. Bacteriol.*  
918 **196**, 4044–4056 (2014).

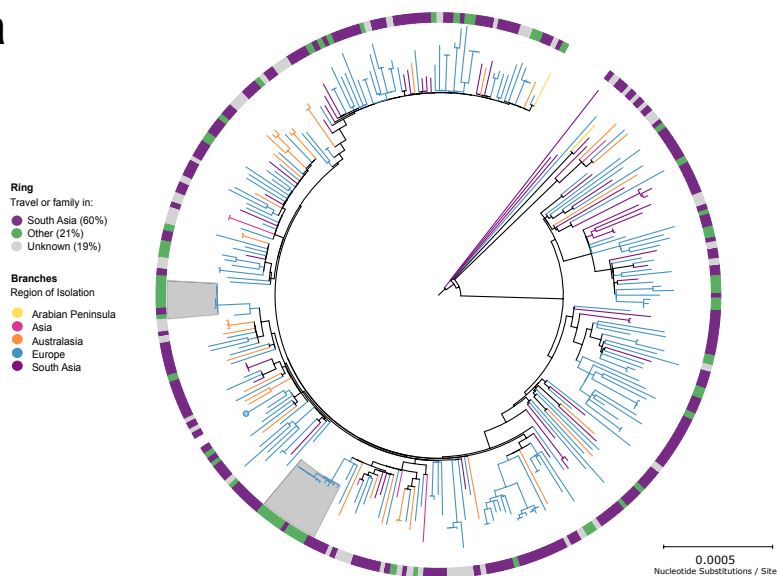
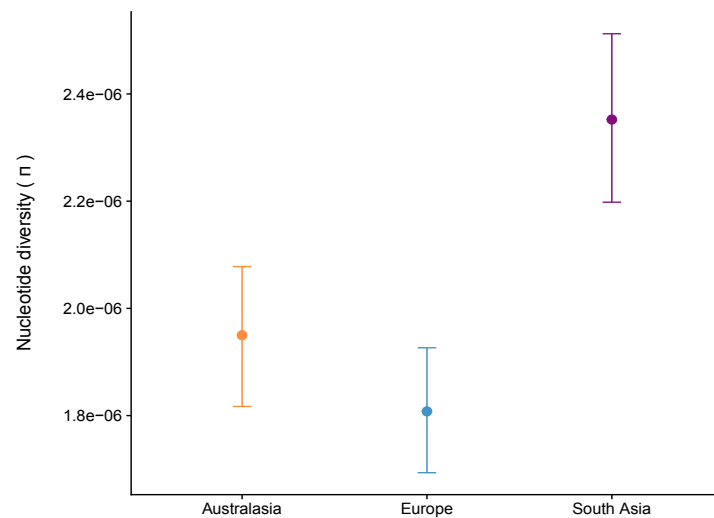
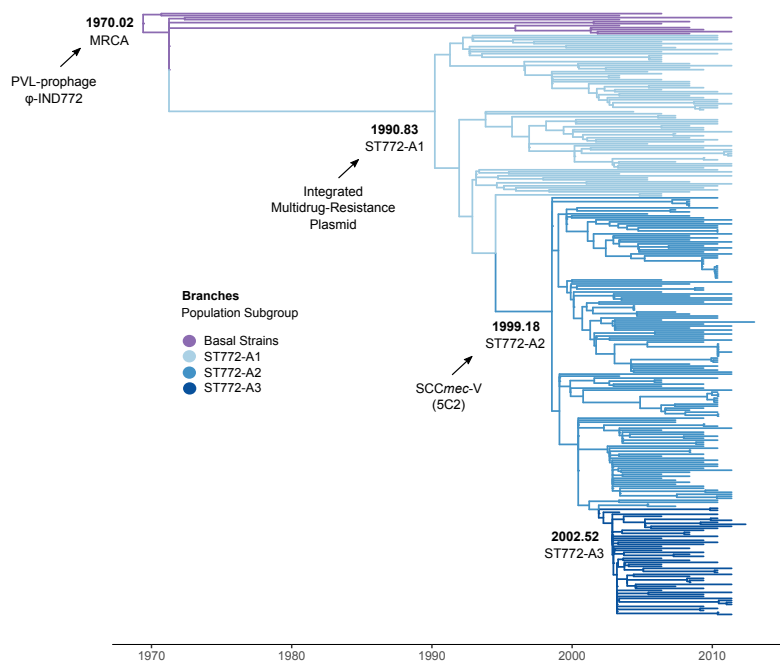
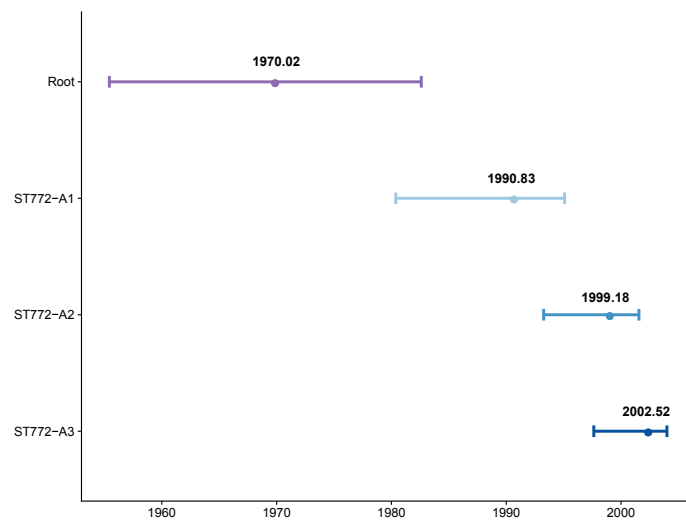
919 90. Ziebuhr, W. *et al.* Detection of the intercellular adhesion gene cluster (*ica*) and phase  
920 variation in *Staphylococcus epidermidis* blood culture strains and mucosal isolates. *Infect.*  
921 *Immun.* **65**, 890–896 (1997).

922 91. Dale, R. *et al.* Bioconda: A sustainable and comprehensive software distribution for the life  
923 sciences. *bioRxiv* (2017).

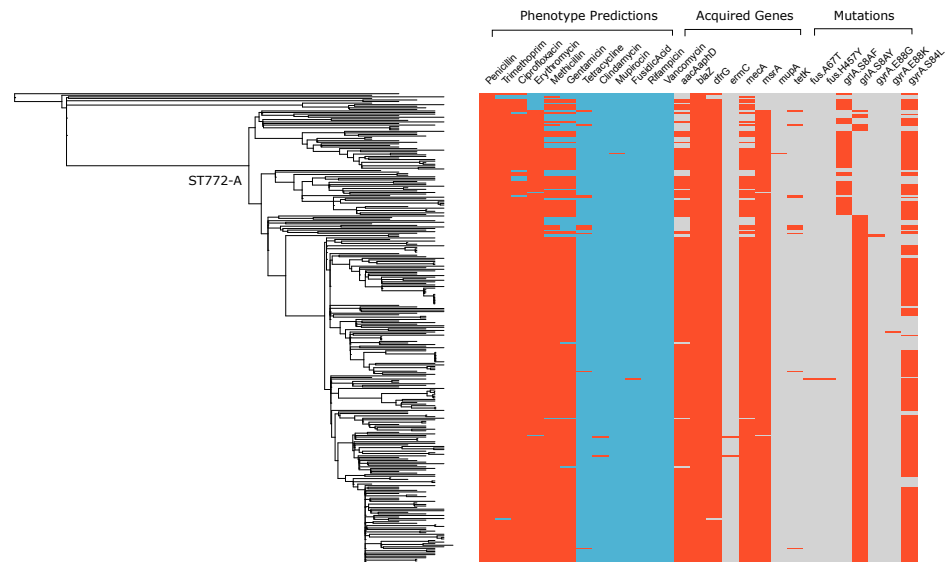
924 92. Köster, J. & Rahmann, S. Snakemake—a scalable bioinformatics workflow engine.  
925 *Bioinformatics* **28**, 2520–2522 (2012).

926

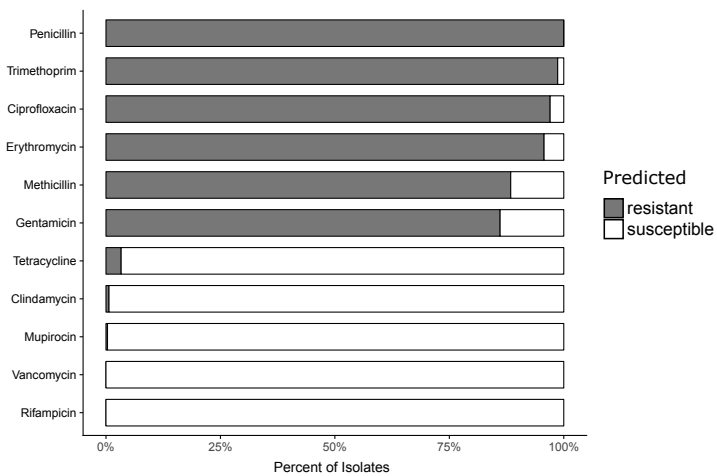


**a****b****c****d**

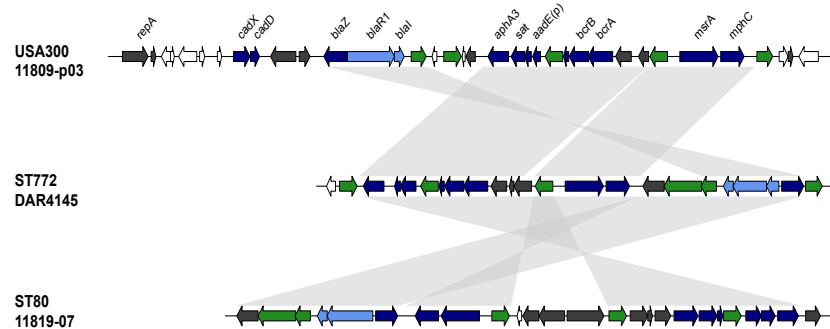
a



b



c



d

